This is a preprint of the following article:
Giostri, A., Romei, A. & Binotti, M., "*Off-design performance of closed OTEC cycles for power generation*", Renew. Energy, 2021.
The published article may differ from this preprint, and is available at the following DOI: 10.1016/j.renene.2021.02.047.

Off-design performance of closed OTEC cycles for power generation

Andrea Giostri*, Alessandro Romei, Marco Binotti

Politecnico di Milano – Dipartimento di Energia
Via Lambruschini 4, 20156 Milano – Italy
Web-site: www.gecos.polimi.it, www.lfm.polimi.it
*corresponding author: ph. +39 02 2399 3892; e-mail: andrea.giostri@polimi.it

Abstract

The present study illustrates the development of a detailed model to estimate the part-load performance of an ammonia closed OTEC system for on-shore installations. A previously published Matlab® suite is extended by accounting for off-design conditions in terms of variable seawater temperature and mass flow on the cycle performance. The off-design behavior of each component is thoroughly discussed, with particular attention devoted to the single-stage axial-flow turbine, whose performance maps are obtained by means of three-dimensional CFD simulations. Assuming a representative plant sized for warm seawater temperature of 28°C and cold seawater temperature of 4°C (8500 kg/s taken from 1000 m depth), the model predicts an annual electricity yield of 15.963 GWh_e and LCOE of 316 €/MWh_e when including seawater measured data of a simile-Hawaiian site. Moreover, a sensitivity analysis is assessed in order to identify the best design parameters (i.e. warm seawater temperature and cold seawater mass flow rate) that minimize the LCOE for the given location. The new design guarantees a reduction of approximately 11% of the LCOE (284 €/MWh_e). The simulation capabilities of the developed model prove it as valuable tool to estimate the OTEC competitiveness in different scenarios.

Keywords: Renewable energy, Ocean Thermal Energy Conversion, OTEC, ammonia cycle, ammonia turbine

Acronyms

CC	Closed Cycle
CFD	Computational Fluid Dynamic
CWP	Cold Water Pipe
HDPE	High density polyethylene
HX	Heat exchanger
FCR	Fixed Charge Rate
LCOE	Levelized cost of electricity
OTEC	Ocean Thermal Energy Conversion
PHES	Pumped Heat Electrical Storage
PV	Photovoltaic
RANS	Reynolds-averaged Navier Stokes
WWP	Warm Water Pipe

Nomenclature

A	Area	m^2
D	Inner diameter	m
H	Head	m
K	Thermal Conductivity	$W\ m^{-1}\ K^{-1}$
L	Length	m
P	Pressure	Pa
Pr	Prandtl number	-
$\dot{Q}$	Thermal power	kW
R	Thermal resistance	$m^2\ K\ W^{-1}$
Re	Reynolds number	-
T	Temperature	K
U	Global heat transfer coefficient	$W\ m^{-2}\ K^{-1}$
$\dot{W}$	Power	kW
d	Depth	m
h	enthalpy	$J\ kg^{-1}$
htc	Heat transfer coefficient	$W\ m^{-2}\ K^{-1}$
l	Specific work	$J\ kg^{-1}$
$\dot{m}$	Mass flow rate	$kg\ s^{-1}$

This is a preprint of the following article:
Giostri, A., Romei, A. & Binotti, M., "*Off-design performance of closed OTEC cycles for power generation*", Renew. Energy, 2021.
The published article may differ from this preprint, and is available at the following DOI: 10.1016/j.renene.2021.02.047.

V	Velocity	m s^{-1}

Greek letters

Δ	Difference	-
β	Expansion ratio	-
γ	Gamma parameter	kW m^{-2}
η	Efficiency	-
μ	Viscosity	Pa s
ρ	Density	kg m^{-3}
σ	Salinity	g l^{-1}
ω	Rotational speed	rpm

Subscripts

cond	Condenser
cr	Critical
cw	Cold water
eul	Eulerian
eva	Evaporator
in	Inlet
is	Isentropic
nom	Nominal conditions
on	On-design conditions
out	Outlet
pp	Pinch-point
r	Reduced quantity
sw	Seawater
T	Turbine
wf	Working fluid
ww	Warm water

1 Introduction

The great consensus among scientific community [1] that identifies global warming to be most likely caused by greenhouse gases emitted by anthropic activities is pushing political actions [2,3] and research in the power generation sector towards carbon-free technologies.

Ocean thermal energy conversion (OTEC), which exploits the thermal gradient between warm surface seawater and cold deep seawater in tropical oceans to generate electricity, is a promising power generation technology that positively responds to the request of increasing the share of renewable energy sources in the electricity generation sector. Although the worldwide OTEC theoretical potential is undoubtedly huge (10 TW without affecting ocean thermal structure [4], its limited development involves higher electricity generation cost than other renewable technologies (i.e. wind, PV) [5]; hence, a complete development of this technology has a vital need to be subsidized. Although the high cost of electricity, which is roughly in the range 0.07 – 0.5 €/kWh_e [6][a], seems to be an unsurmountable hurdle to the affirmation of OTEC technology, remote islands and archipelagos characterized by a significant thermal gradient (i.e. 20°C - 25°C) can be suitable scenarios for OTEC installations, replacing the conventional source of electricity given by Diesel gensets that use high fuel costs (because of high transportation distance)[b]. In addition, as stated in [6,7], the competitiveness of OTEC can be further enhanced by the potential revenue (i.e. carbon tax) derived from the reduction of emitted CO_2 compared to conventional fossil fueled Diesel genset [7]. Additionally, an important peculiarity of OTEC technology is represented by its inherent capability to be adapted to different load sizes, ranging from MW to hundreds MWs, thus widening the number of people that can access to renewable energy.

Following the previous study published by the authors [8], this paper focuses on the performance prediction of an ammonia saturated CC-OTEC (Closed cycle OTEC) in a scenario characterized by variable seawater conditions. The choice of saturated Rankine cycle is recognized as a good compromise between plant simplicity (investment cost) and conversion efficiency. Many CC-OTEC variants have been proposed (i.e. Kalina cycle, Uehara cycle, multi-stage configuration etc.) [9-12] but, although attaining higher conversion efficiency, their superiority, in terms of cost of electricity, has not been

[a] The wide cost range of electricity is caused by different economic assumptions and plant size investigated in literature.

[b] Gensets operating in remote islands are dated or have exceeded the manufacturers recommended lifespan [7].

This is a preprint of the following article:
Giostri, A., Romei, A. & Binotti, M., "*Off-design performance of closed OTEC cycles for power generation*", Renew. Energy, 2021.
The published article may differ from this preprint, and is available at the following DOI: 10.1016/j.renene.2021.02.047.

plainly proved. The working fluid selection is driven by the research findings reported in Open Literature [13] that clearly identify ammonia as the best working fluid for a plants size of the order of MWs.
An in-house code was developed to study the part-load behavior of CC-OTEC system. Moreover, the modeling tool in conjunction of a procedure to size the overall plant can be effectively used to predict the OTEC economic competitiveness through Levelized Cost of Electricity (LCOE) estimate. It is worth to underline that, in most of the studies present in literature, the off-design behavior of CC-OTEC is marginally treated or even neglected, hence reducing the reliability of the computed annual electricity yield. Although for specific sites that feature small seawater temperature variabilities a simple optimization at nominal conditions can be justified, in most of the cases it may potentially fail to predict the best techno-economic solution. In this paper, we provide some numerical evidences by re-assessing the design parameters in light of its off-design behavior, showing that they can be properly selected to achieve the minimum LCOE.
After describing the methodology adopted (section 2), in terms of developed tools and performed analyses, the design parameters of a representative OTEC design, which is used to verify the capabilities of the part-load model, are resumed (section 3). Then, the off-design model is detailly described (section 4) with particular attention posed on both the description of the equations that model the components behavior and the discussion of off-design system performance. Considering the time series of seawater data, both the annual energetic and economic figure of the OTEC plant is assessed (section 5). Furthermore, different OTEC system designs are investigated. Finally, the conclusions and a list of future developments are drawn (section 6).

2 Methodology

In case of significant variations of the seawater temperature (mainly the superficial temperature) during the year, OTEC plant optimization considering design conditions only can be not sufficient. As a matter of fact, the evaluation of the technology attractiveness can be biased by an additional uncertainty related to the net electricity output estimate. For this reason, a dedicated model able to simulate part-load conditions can play an important role in offering a more complete plant assessment.
In order to positively response to this need, a CC-OTEC off-design model is coded in Matlab® [14], extending the design code previously developed by the authors [8] that did not consider any seawater temperature variation during time.
In the first part of the proposed study, the off-design model is described and discussed with particular attention posed on the discussion of the governing equations that describe each component behavior. Within these circumstances, there are no previous works in Open Literature that provide detailed information on the part-load behavior of an ammonia turbine tailored for CC-OTEC power systems. To this end, first a preliminary 3D design of the turbine is carried out based on a mean-line representation, then it is analyzed via three-dimensional CFD simulations to derive complete performance maps that are crucial to obtain a reliable cycle part-load assessment.
Once the modelling approaches of each component are discussed, the developed tool is used to study the response of a given OTEC plant [8] to variable operating conditions. Subsequently, the annual electricity yield for a selected plant location, which is characterized by time series of both warm and cold seawater temperature, is estimated. Once the yearly electricity output is known, the LCOE is computed considering the components' investment and O&M costs.
The second part of the study aims at extending the CC-OTEC analysis presented in the previous work [8], which involves a CC-OTEC design optimization based on a single value of cold seawater mass flow rates (i.e. 8500 kg/s) and warm seawater temperature (i.e. 28°C). In particular, several designs that differ in both cold seawater mass flow rates and warm seawater temperature are defined and the LCOE is estimated. Through this sensitivity analysis, the best OTEC design characterized by the lowest LCOE is identified.
Figure 1(a) shows the CC-OTEC plant layout based on an ammonia saturated Rankine cycle where warm and cold seawater are pumped and sent to the power block via dedicated pipes, namely cold seawater pipe (CWP) and warm seawater pipe (WWP). In addition, the components and streams number, used in the following sections, are reported. Figure 1(b) graphically explains the proposed methodology for the investigation of the OTEC performance (both from an energetic and economic point of view), explicitly listing the model inputs required to accurately model the system; moreover, the interactions among sub-models are reported as well. Focusing on the red square, which represents the off-design model, design characteristics of each component are required as input. In particular, components size (i.e. heat exchanges area, seawater pipes sizes) and nominal operating parameters (i.e. heat transfer coefficients, pressure drops, efficiencies, expander performance map) are retrieved from the design model, while components equations (i.e. energy balance, turbine performance map, heat transfer correlations etc.), which model off-design behavior, are added. The system performance map, expressed as function of seawater mass flows and temperatures, obtained from the off-design model, is then used for the annual simulation to obtain the annual electricity yield and LCOE after having prescribed the seawater temperatures evolution in time, the economic assumptions (i.e. components specific cost, discount rate etc.) and component sizes.
As regards the design tool [8], given the cold mass flow (m_{cw}) and the seawater temperatures (T_{cw},T_{ww}) along with the components main assumptions, it is able to find the minimum temperature difference of both condenser ($\Delta T_{pp,ww}$) and evaporator ($\Delta T_{pp,cw}$) along with the temperature difference of both seawater streams (ΔT_{cw}, ΔT_{ww}) that guarantee the maximum ratio between net power output and total heat exchangers area, defined as γ parameter, widely adopted in OTEC research [15,16]. The sizing of plate heat exchangers (PHX) is performed through the choice of seawater the velocity in the channels (v_{HX}).

This is a preprint of the following article:
Giostri, A., Romei, A. & Binotti, M., "*Off-design performance of closed OTEC cycles for power generation*", Renew. Energy, 2021.
The published article may differ from this preprint, and is available at the following DOI: 10.1016/j.renene.2021.02.047.

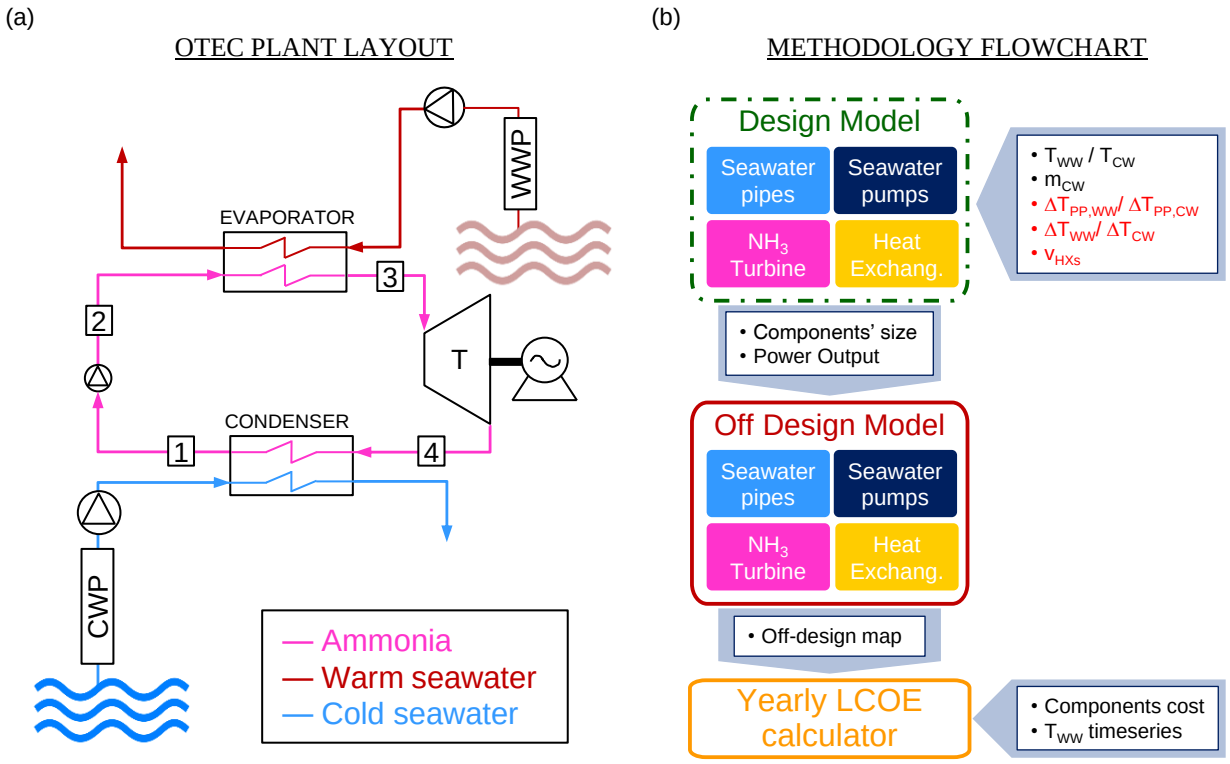

Figure 1 Layout of the CC-OTEC system (a). Scheme of the methodology adopted in the development of the OTEC model (b).

The external NIST-REFPROP routines [17] are used to compute the thermodynamic properties of ammonia; for this working fluid, the NIST-REFPROP implements a multi-parameter equation of state expressed in terms of Helmholtz fundamental relation [18]. Seawater properties are computed by TEOS-10 equations of state [19].
In the next section, alongside the modelling approach, the governing equations are reported, highlighting the main assumptions.
The proposed methodology has a greater impact in sites characterized by a significant time-varying superficial seawater temperature such as the hypothetical Hawaiian site chosen for this study. This peculiarity is neither unique nor rare but can be easily found in many other sites.
For example, Kumejima Island (Japan) [20], where a 100 kW_e plant has been operating since 2013, is characterized by approximately 10°C span in warm seawater temperature during year. On the contrary, a fair study cannot avoid reporting that other promising sites have seawater temperature nearly constant during time (maximum oscillation smaller than 2°C) like, for example Guam island [21].

3 Design condition

The first step necessary to analyze the OTEC system performance is represented by the identification of the system design. With the purpose of explaining the implemented model, OTEC plant characteristics are derived from [8], to which the reader is indexed to have a more detailed discussion. The considered OTEC system is sized assuming cold and warm seawater temperature equal to 4°C and 28°C, respectively, and considering seawater pipes diameter equal to 2.5 m, a value that can be considered as the current technological limit of HDPE (High density polyethylene) pipes [22]. The cold mass flow rate is set to 8500 kg/s.
All the assumptions related to the system design along with the main design parameters are reported in Table 1.

Table 1 Resume of on-design characteristics of the OTEC plant [8].

On-design parameters		
	Symbol	Value
Seawater flows		
Warm/Cold seawater temperature, °C	T_{ww}, T_{cw}	28, 4
Warm/Cold seawater mass flow rate, kg/s	$\dot{m}_{ww}$, $\dot{m}_{cw}$	8798, 8500
Seawater salinity, g/l	σ	35

This is a preprint of the following article:
Giostri, A., Romei, A. & Binotti, M., "*Off-design performance of closed OTEC cycles for power generation*", Renew. Energy, 2021.
The published article may differ from this preprint, and is available at the following DOI: 10.1016/j.renene.2021.02.047.

Seawater pipes		
Diameter of cold/warm water pipe, m	D_{CWP}, D_{WWP}	2.5
Length of cold/warm water pipe, m	L_{CWP}, L_{WWP}	3000, 200
Depth of cold water, m	d_{CWP}	1000
Turbomachinery efficiency		
Ammonia turbine isentropic efficiency,	$\eta_{is,T}$	0.890
Ammonia pump isentropic efficiency,	$\eta_{is,pump}$	0.850
Ammonia turbine mechanical efficiency,	$\eta_{mech,T}$	0.985
Ammonia pump mechanical efficiency,	$\eta_{mech,T}$	0.970
Ammonia pump electric efficiency,	$\eta_{el,pump}$	0.970
Generator electric efficiency,	$\eta_{el,T}$	0.980
Hydraulic efficiency of seawater pumps,	$\eta_{hyd,sw,pump}$	0.850
Seawater pumps mechanical efficiency,	$\eta_{mech,sw,pump}$	0.970
Seawater pumps electric efficiency,	$\eta_{el,sw,pump}$	0.970
Ammonia turbine		
Mass flow, kg/s	$\dot{m}_3$	92.8
Inlet pressure, bar	P_3	9.15
Inlet temperature, °C	T_3	22.1
Expansion ratio,	β	1.42
Outlet temperature, °C	T_4	11.3
Rotational speed, rpm	ω_{rpm}	3000
Heat exchangers		
Overall heat transfer coeff. of evaporator/condenser, W/m^2/K	U_{eva}, U_{cond}	4019.4, 3464.7
Heat exchange area of evaporator/condenser, m^2	A_{eva}, A_{cond}	6646.9, 7478.6
Seawater pressure drop of evaporator/condenser, bar	$\Delta P_{sw,eva}$, $\Delta P_{sw,cond}$	0.4221, 0.3704
System performance		
Net power output, kW$_e$	W_{net}	2356.2
Power consumption warm/cold seawater pump, kW$_e$	W_{ww}, W_{cw}	481.7, 1038.8
Net efficiency,	η_{net}	0.0206

4 Off-design modelling

As regards the parameters that influence the OTEC system behavior, the exogenous parameters are the cold and warm seawater temperature (T_{ww} and T_{cw}). These temperatures show variations during time that strongly depend on the plant location. Warm seawater is undoubtedly characterized by more sensible oscillations than cold (deep) seawater. The effect of seawater salinity change is neglected.
The OTEC plant has to face change of seawater temperatures, dealing with off-design operation that has to be properly considered to get a reliable estimate of the plant profitability.
The modelled OTEC system can vary the seawater pumps rotational speed thanks to their variable speed drive, in order to guarantee the maximum net power output for any given seawater temperatures. This degree of freedom could also be exploited to follow the electricity load requested. Anyhow, it is important to stress that OTEC plants offer a slow response to load change because of their significant heat exchangers' thermal inertia.
As regards the net power output constraints, maximum and minimum net power output are limited to 1.15 and 0.15 of the design values respectively.
The developed algorithm computes off-design performance taking into account the characteristic equations of each components coupled with the operational constraints. The resulting set of non-linear equations is solved with KINSOL [23,24].
In the following, the characteristic equations of the system components are reported and discussed. It is worth to underline that particular attention is devoted to the ammonia turbine whose main characteristics (i.e. isentropic efficiency and operation map) are detailly investigated.

4.1 Turbine

A preliminary turbine sizing was carried out with an in-house mean-line code [25,26]. The mean-line flow representation assumes unidirectional and uniform flow along the midspan direction, relying on semi-empirical correlations for loss

This is a preprint of the following article:
Giostri, A., Romei, A. & Binotti, M., "*Off-design performance of closed OTEC cycles for power generation*", Renew. Energy, 2021.
The published article may differ from this preprint, and is available at the following DOI: 10.1016/j.renene.2021.02.047.

estimates and angle deviations. The turbine boundary conditions, mass flow rate and rotational speed were assigned to comply with the design requirements of the ammonia power cycle, detailed in section 3. The limited pressure ratio imposed by the power cycle can be effectively realized in a single-stage turbine, thus guaranteeing a relevant technical simplification. The number of blades was estimated with a well-established loading criterion [27], yielding 67 and 71 blades for the stator and rotor, respectively. The turbine efficiency, expressed hereinafter as:

$$\eta_T = \frac{l_{eul}}{h_{T3} - h_{4is} - 0.5\, v_{out}^2/2}, \tag{1}$$

where half of the outlet kinetic energy was assumed to be recovered with a diffuser [28], was the objective function of a dedicated optimization task based on differential evolution algorithm [29]. As a result of the optimization procedure, a first estimate of main geometrical parameters was obtained. An additional refinement of the geometry was carried out in light of the preliminary CFD results, ultimately yielding to the final turbine sizing sketched in Figure 2. To ease the blade manufacturability, dihedral blades were used for both the stator and rotor, extruding the midspan blade profiles along the whole span. The resulting reaction degree of the machine was approximately 0.5, in agreement with standard design practices for maximum efficiency operation. In the following, CFD simulations of such turbine design are performed to generate comprehensive off-design performance maps, which will be embedded in the cycle off-design routine.

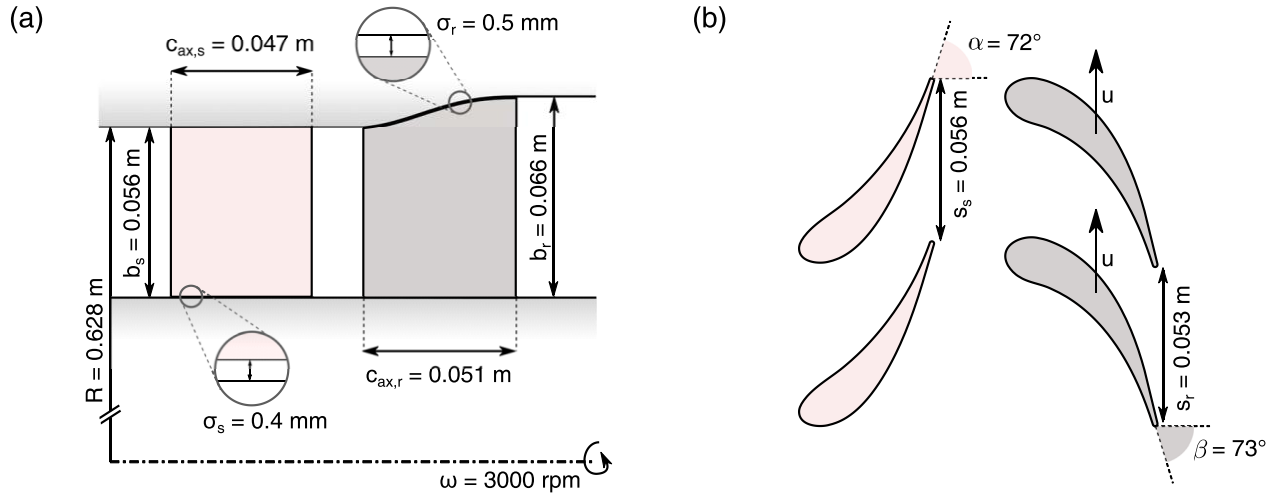

Figure 2 Main geometrical parameters of the axial-flow single-stage ammonia turbine reported in the (a) meridional plane and (b) blade-to-blade plane at midspan.

4.1.1 Computational flow solver

Steady Reynolds-averaged Navier Stokes (RANS) equations were solved with the commercial software ANSYS-CFX 18.1® [30]. The total pressure and total temperature, along with an axial flow direction, were assigned as boundary conditions at the stator inlet, while the static pressure was imposed at the rotor outlet. A mixing-plane interface that circumferentially averages velocity components was placed between the stationary and the rotating domain, thus permitting the simulation of a single blade passage for both the stator and rotor by imposing periodic boundary conditions. To avoid spurious pressure oscillation at the stator-rotor interface in off-design conditions, the stator-rotor axial gap was increased to one stator axial chord. Besides improving the convergence, the increased stator-rotor gap is not supposed to affect the performance estimates as steady simulations are inherently unable to predict the unsteady stator-rotor interaction. This latter contribution is however expected to be small owing to the low-loaded stage. Finally, no-slip and adiabatic boundary conditions were supplied to the blade walls and endwalls (hub and shroud).

RANS equations were complemented with the two-equation turbulence model k − ω SST [31], which was implemented in the flow solver so that it automatically switches from solving the turbulence equations near the wall to introducing wall-functions in the solution depending on the local y^+ value. The Reynolds number of the cascade was high enough $Re > 10^6$ to justify fully turbulent flows. A turbulence intensity equal to 5% and an eddy-to-molecular viscosity ratio equal to 5 were assigned as inlet boundary conditions in all simulations. For both flow and turbulence equations, advective terms were solved with a high-resolution numerical scheme, while a central-difference scheme was employed for viscous terms.

Although the expansion process falls within the saturation dome, single-phase simulations were carried out by extrapolating single-phase properties till the spinodal limit [32]. From a physical perspective, the underlying assumption is that non-equilibrium effects dominate, thus permitting the penetration of the single-phase vapor into the meta-stable region without undergoing to a phase change. Within this framework, potential additional losses related to phase change phenomena were neglected when determining the machine efficiency [33]. Thermodynamic properties were incorporated

This is a preprint of the following article:
Giostri, A., Romei, A. & Binotti, M., "*Off-design performance of closed OTEC cycles for power generation*", Renew. Energy, 2021.
The published article may differ from this preprint, and is available at the following DOI: 10.1016/j.renene.2021.02.047.

into a look-up table approach by using pressure and temperature as primitive variables. The table ranges were taken large enough to avoid any clips or extrapolations which may make critical the convergence process, with an accuracy of approximately 0.1 K and 0.1 bar for temperature and pressure, respectively. A finer thermodynamic discretization did not lead any substantial variation in solution.

Meshes were composed by structured hexahedral elements, realized with ANSYS-TURBOGRID®. A local cell clustering was imposed near blade walls to obtain $y^+ \approx 1$, thus properly solving the boundary layer on the blades. A coarser cell refinement was applied at the endwalls to alleviate the computational burden, resulting in $y^+ \approx 30$ therein. Although the introduction of wall functions at the endwalls might potentially cause an underestimation of secondary losses, this latter contribution was expected to be limited because of the comparatively low stage loading.

A dedicated grid-convergence study is reported in Figure 3 (a) with five grid refinements. Specifically, stator and rotor meshes were obtained by doubling the overall cell number each time, both starting from approximately 4.3×10^5 cells with around 9.2×10^3 elements in the blade-to-blade plane. Regardless of the level of refinement, each mesh retained the cell distribution at the walls that was previously discussed. A grid-independent turbine efficiency, following the definition in Equation (1), is obtained after four refinement, yielding similar meshes for the stator and rotor, which are roughly composed by 3.5×10^6 elements with 4.0×10^4 elements in the blade-to-blade plane, respectively. The grid-independent mesh is reported in Figure 3(b) for both the stator and rotor passages.

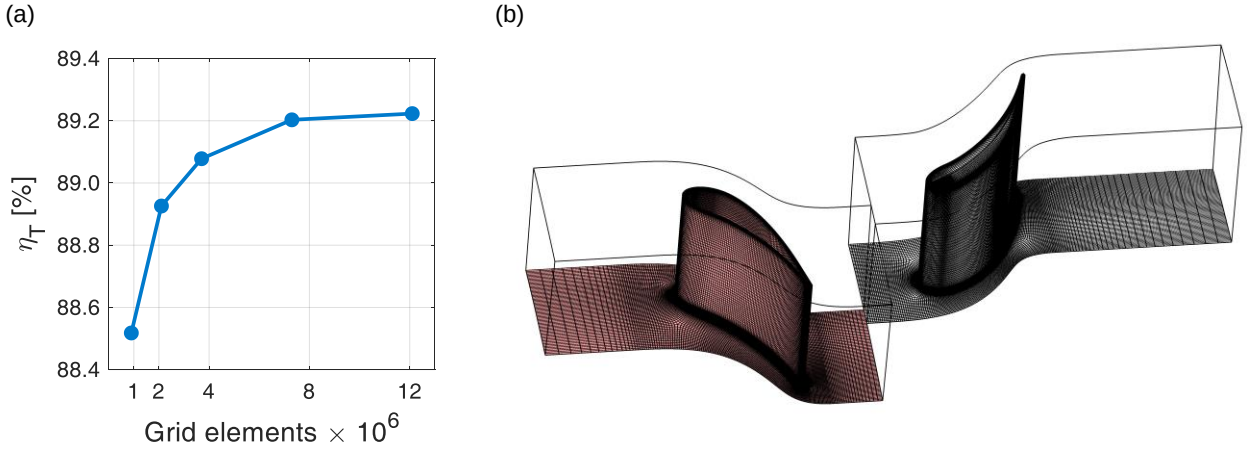

Figure 3 Grid-convergence assessment in terms of turbine efficiency (a) and grid-independent mesh selected for the generation of off-design performance maps (b).

4.1.2 Turbine aerodynamics and off-design performance maps

The flow field of the single-stage ammonia turbine at design conditions, setting $P_T = 9.15$ bar and $T_T = 22.1$ °C at the inlet (corresponding to saturated vapor at that temperature) and $P = 6.17$ bar at the outlet, is reported in Figure 4. The resulting design pressure ratio is $\beta = 1.5$. The flow regime is subsonic everywhere, with a Mach number at the throat approximately $M = 0.5$, which raises up to $M = 0.7$ on the rear suction side. The rotor incidence is almost null at the midspan, confirming the quality of the preliminary design based on mean-line considerations. As a consequence of the two-dimensional rotor evolution along the span, slightly positive and negative incidence angles up to $\pm 5°$ are found at the rotor hub and shroud, respectively, with a limited impact on the overall efficiency, which is $\eta_T = 89.2\%$.

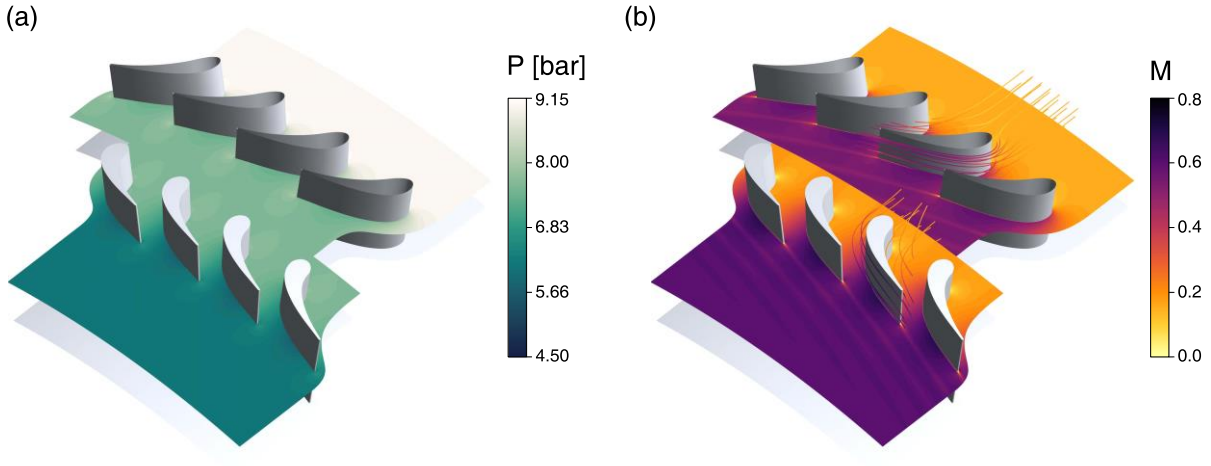

Figure 4 Flow field expressed in terms of (a) pressure and (b) absolute and relative Mach number for stator and rotor, respectively, at cycle nominal conditions.

This is a preprint of the following article:
Giostri, A., Romei, A. & Binotti, M., "*Off-design performance of closed OTEC cycles for power generation*", Renew. Energy, 2021.
The published article may differ from this preprint, and is available at the following DOI: 10.1016/j.renene.2021.02.047.

Off-design performance maps, reported in Figure 5 both in dimensional and dimensionless form, are generated by varying the outlet pressure while freezing the upstream total state that corresponds to a specific saturated vapor condition. The rotational speed is kept constant at $\omega = 3000\ rpm$. The procedure is repeated for different saturated temperature levels at the turbine inlet. Each curve is built on the basis of five separate CFD runs. An additional CFD simulation is performed for the intermediate temperature level to have a more realistic interpolation of the dimensionless efficiency curve close to the peak value. As previously noted, both the stator and rotor operate in a subsonic regime with a Mach number below unity at the throat, thus far from choked conditions, which are instead reached simultaneously in both cascades (as the overall expansion ratio is almost equally split between the stator and rotor) when the overall turbine pressure ratio exceeds $\beta_{cr} \gtrsim 2.0$. Notice that the critical expansion ratio is lower than its counterpart for steam and gas turbines because the operating temperature is significantly reduced, hence exhibiting a lower speed of sound in such thermodynamic conditions. In the range of interest circumscribed by the seasonal variability of the seawater temperature, the turbine never operates in choked conditions because the associated pressure ratio is always lower than the critical one. The efficiency trend is almost constant in the neighborhood of the design point ($0.85 < \dot{m}/\dot{m}_{nom} < 1.00$), then suddenly dropping at lower and higher flow rate mainly due to a variation of the flow angle at the rotor leading edge, provoking a flow separation on the pressure and suction side, respectively. Following the efficiency definition provided in Eq. (1), it is not surprising that the turbine efficiency can slightly increase ($\Delta\eta_T = +0.35\%$) at flow rates lower than the design one ($\dot{m}/\dot{m}_{nom} \approx 0.95$) because the associated reduction in the outlet kinetic energy overcomes the increase in fluid-dynamic losses.
The performance maps are generalized by recalling the standard definition of reduced mass flow rate:

$$\dot{m}_r = \dot{m}\frac{\sqrt{T_{in}}}{P_{in}}, \tag{2}$$

Although Equation (2) is strictly valid only for ideal-gas flow [34], real-gas effects can be practically neglected since the compressibility factor approaches unity ($Z \approx 0.9$ in all expansion processes under examination). Moreover, from Figure 5 it can be clearly noticed that all dimensional curves, parametrized in terms of saturated temperature at the turbine inlet, collapse in a single dimensionless curve for both the pressure ratio and efficiency against the reduced mass flow rate. This evidence can be explained by referring to the similitude theory: given the same pressure ratio, the considered temperature variations do not entail appreciable differences in the fluid thermophysical properties (the ratio among specific heats is nearly constant), hence the machine loading is in practice constant. Moreover, the Reynolds number is sufficiently high (Re >10^6) in all expansion processes to ensure self-similarity in Reynolds effects. Finally, the evolution of the speed of sound, hence the Mach number at a given stage loading, is the same regardless of the inlet temperature level. In this context, the similitude theory holds, as further confirmed by the flow simulations that were carried out in this work

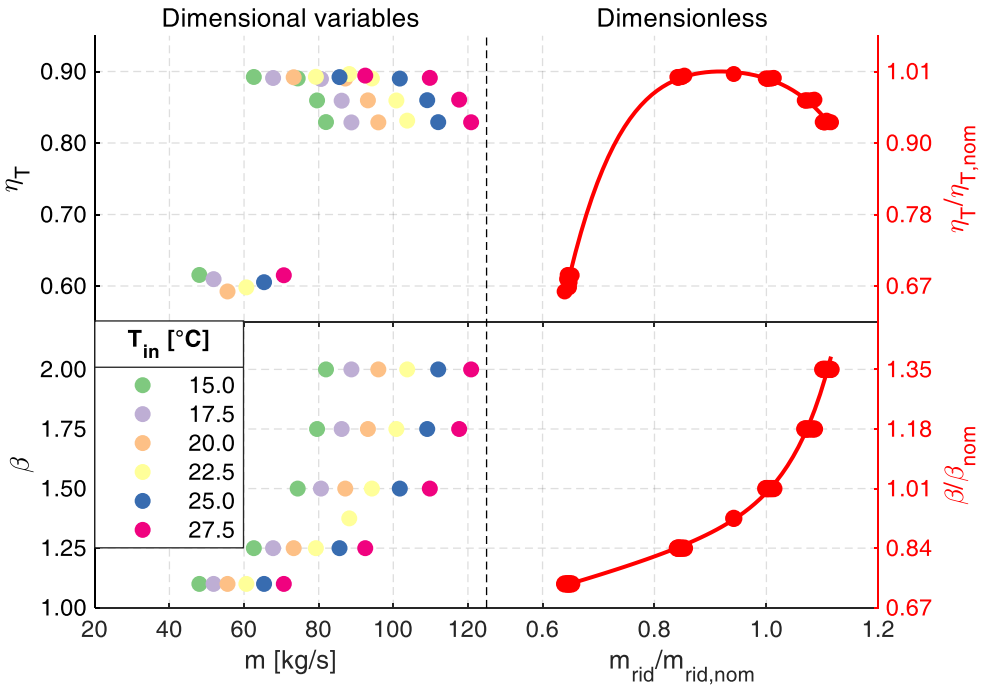

Figure 5 Performance maps of the single-stage axial-flow ammonia turbine.

The expansion ratio and the isentropic efficiency, expressed in dimensionless from, are approximated by two analytical functions, thus simplifying their usage in future studies:

This is a preprint of the following article:
Giostri, A., Romei, A. & Binotti, M., "*Off-design performance of closed OTEC cycles for power generation*", Renew. Energy, 2021.
The published article may differ from this preprint, and is available at the following DOI: 10.1016/j.renene.2021.02.047.

$$\frac{\beta}{\beta_{nom}} = A_\beta e^{B_\beta\left(\frac{m_r}{m_{r,nom}}\right)} + C_\beta e^{D_\beta\left(\frac{m_r}{m_{r,nom}}\right)}, \quad (3)$$

$$\frac{\eta}{\eta_{nom}} = A_\eta\left(\frac{m_r}{m_{r,nom}}\right)^4 + B_\eta\left(\frac{m_r}{m_{r,nom}}\right)^3 + C_\eta\left(\frac{m_r}{m_{r,nom}}\right)^2 + D_\eta\left(\frac{m_r}{m_{r,nom}}\right) + E_\eta, \quad (4)$$

The numerical coefficients (A, B, C, D and E) are determined via a least-square regression and they are explicitly reported in Table 2.

Table 2 Coefficients used in the functions for the calculation of the off-design expansion ratio and efficiency.

	Coefficients				
	A	B	C	D	E
β	0.494	0.6259	5.403E-8	14.16	-
η	-27.45	103.52	-147.96	94.89	-22.00

Since the ammonia expander does not have a partial-admission stage, the sliding pressure mode, which allows the turbine inlet pressure to freely change with load, is considered.

4.2 Heat exchanger

In off-design conditions, the change of ammonia and seawater mass flows together with the change of fluids thermophysical properties directly impact on the convective heat transfer coefficient. The nominal overall heat transfer coefficient (U_{nom}) of the Plate Heat Exchangers (PHX) is estimated with the Aspen® EDR [35]. Taking into account the PHX structure, the overall heat transfer coefficient is made of three contributions, namely, the convective heat transfer coefficient of both the working fluid (htc_{wf}) and the seawater side (htc_{sw}), and the wall conductive resistance (R''_{wall}) as reported in the following relation:

$$U = \left(\frac{1}{htc_{wf}} + \frac{1}{htc_{sw}} + R''_{wall}\right)^{-1} \quad (5)$$

Table 3 reports the nominal overall heat transfer coefficients for both evaporator and condenser [8] and the ratios between U_{nom} and the three considered thermal resistances contributions reported above, namely, α_{sw}, α_{wf}, and α_{wall}.

Table 3 Sizing performance of HX.

Sizing performance of HX			
	Symbol	EVA	COND
Overall heat transfer coefficient, W/(m^{2}K)	U_{nom}	4019.4	3464.7
Seawater convective resistance/total resistance,	α_{sw}	0.4517	0.4355
Ammonia convective resistance/total resistance,	α_{wf}	0.1263	0.1089
Wall resistance/total resistance,	α_{wall}	0.4220	0.4556

The main parameters that influence the overall heat transfer coefficient are taken into account to estimate the PHX performance in off-design conditions. In particular, Cooper's correlation [36,37] is implemented to model the ammonia evaporation in part-load operation, resulting in the following expression for the overall heat transfer coefficient (U_{EVA}):

$$U_{EVA} = \frac{1}{\frac{\alpha_{sw}}{U_{nom}\left(\frac{\dot{m}_{sw}}{\dot{m}_{sw,on}}\right)^{0.6}} + R''_w + \frac{\alpha_{wf}}{U_{nom}\left[\left(\frac{p_{red}}{p_{red,on}}\right)^{0.12}\left(\frac{-\mathrm{Log}_{10}\,p_{red}}{-\mathrm{Log}_{10}\,p_{red,on}}\right)^{-0.55}\right]^{3.03}}}, \quad (6)$$

where p_{red} is the ratio between the operating pressure and the ammonia critical pressure (113.0 bar) [17].
The condenser overall heat transfer coefficient (U_{COND}) in off-design conditions can be evaluated with the correlation proposed by Kakaç et al. [38]:

This is a preprint of the following article:
Giostri, A., Romei, A. & Binotti, M., "*Off-design performance of closed OTEC cycles for power generation*", Renew. Energy, 2021.
The published article may differ from this preprint, and is available at the following DOI: 10.1016/j.renene.2021.02.047.

$$U_{COND} = \frac{1}{\frac{\alpha_{sw}}{U_{nom}\left(\frac{\dot{m}_{sw}}{\dot{m}_{sw,on}}\right)^{0.6}} + R"_w + \frac{\alpha_{wf}}{U_{nom}\left(\frac{\dot{m}_{wf}\,\mu_{wf,on}}{\dot{m}_{wf,on}\,\mu_{wf}}\right)^{0.8}\left(\frac{Pr_{wf}}{Pr_{wf,on}}\right)^{0.4}\frac{k_{wf}}{k_{wf,on}}\left(\frac{0.55+\frac{2.09}{p_{red}^{0.38}}}{0.55+\frac{2.09}{p_{red,on}^{0.38}}}\right)}}, \quad (7)$$

where Pr_{wf}, k_{wf} and μ_{wf} are the Prandtl number, the thermal conductivity and the dynamic viscosity of the ammonia (saturated liquid).
As far as the seawater pressure drop is concerned, assuming a negligible variation of the friction factor, the off-design pressure drop, for both warm (evaporator) and cold seawater side (condenser), is:

$$\Delta P_{HX,sw,off} = \Delta P_{HX,sw,on}\frac{\left(\dot{m}_{sw}{}^2/\rho_{sw}\right)_{off}}{\left(\dot{m}_{sw}{}^2/\rho_{sw}\right)_{on}}, \quad (8)$$

where ρ_{sw} is the seawater density.

4.3 Seawater pipe

The head losses of seawater pipes strongly affect the seawater pumps consumption. In particular, the change of both seawater mass flow rates and density, which is induced by a temperature change, needs to be taken into account with the relations reported in [15,39,40].As regards the contribute of friction head losses ($\Delta H_{sw,pipe}$), it is assumed to be dependent on seawater velocity solely (for both cold and warm seawater):

$$\Delta H_{sw,pipe} = 6.82\frac{L_{pipe}}{D_{pipe}^{1.17}}\left(\frac{v_{pipe}}{100}\right)^{1.85} \quad (9)$$

Both cold and warm seawater pipe diameters are set to 2.5 m in order to not overcome the limitations imposed by mechanical stresses. [39]. The effect of localized pressure drops (i.e. valves, bends, section changes etc.) is neglected.
As regards the cold seawater pipe, the contribution to head losses of density difference ($\Delta H_{\rho,c}$), which can vary during time, is expressed as follows:

$$\Delta H_{\rho,c} = d_{CWP} - \frac{1}{\rho_{cw}}\left(\frac{1}{2}(\rho_{cw}+\rho_{ww})d_{CWP}\right) \quad (10)$$

4.4 Pumps

As underlined in section 3, seawater pumping power represents about 64% of the system net power output. The pumps consumption mainly depends on the processed mass flow rate, which influences the pressure drop in both heat exchangers and pipes, and, secondarily, on the seawater temperatures (see. 4.3). The electric motor efficiency (η_{el}) and mechanical efficiency (η_{mech}) as function of the load are taken from Thermoflex® [41] and reported in Figure 6. The pumps hydraulic efficiency (η_{hyd}) is assumed constant thanks to the use of a variable speed drive, commonly adopted in axial (or mixed-flow) pumps.

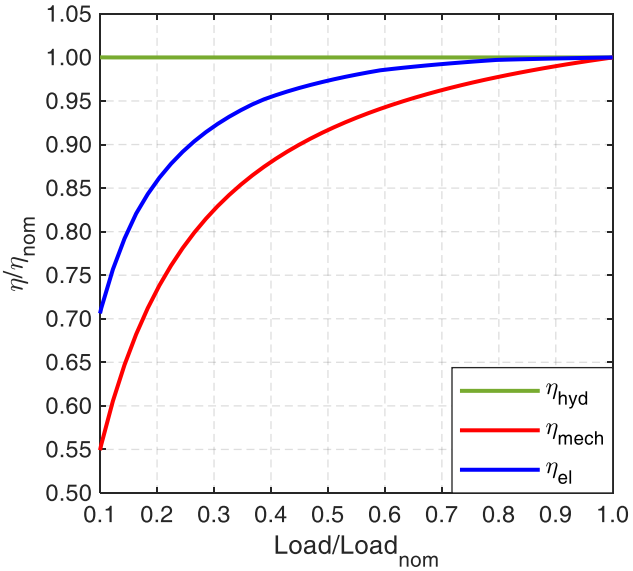

Figure 6 Hydraulic, mechanical and electric efficiency variation as function of load ratio [41].

As regards the ammonia pump, a variable speed drive is assumed as well, thus the same efficiency variations described

This is a preprint of the following article:
Giostri, A., Romei, A. & Binotti, M., "*Off-design performance of closed OTEC cycles for power generation*", Renew. Energy, 2021.
The published article may differ from this preprint, and is available at the following DOI: 10.1016/j.renene.2021.02.047.

above are adopted.

4.5 Off-design results

Once the design characteristics are defined (see section 3), for each value of exogenous parameters (seawater temperatures) and control variables (seawater mass flow rates) the off-design condition can be determined by the model discussed in the sections before. It is important to notice that the two mass flow rates can be varied independently, but for a given cold seawater mass flow rate exists a single value of hot seawater mass flow rate that maximizes the plant net power.
Table 4 reports the system parameters that characterize two representative off-design conditions with respect to the design one (DESIGN). CASE A is characterized by the same seawater temperatures of design case (i.e. 28°C, 4°C) and by a 50% reduction of both seawater mass flow rates. In particular, this condition simulates a wanted load reduction (approximately 84% of nominal load), e.g. to fulfill a hypothetical power change required by the electricity network (if OTEC plant is not used as base-load plant). The decrease of the evaporation temperature and the increase of the condensation temperature causes a drop in cycle efficiency along with a decrease of both turbine pressure ratio and ammonia mass flow rate. It is worth to underline how the turbine isentropic efficiency shows a small increase.
CASE B shows a relevant reduction of the exploitable temperature difference that decreases from 24°C to 17°C. In order to guarantee the maximum net power output, seawater mass flow rates are reduced by the system so that a trade-off between cycle power output and seawater pumps consumption is achieved. Turbine isentropic efficiency shows a limited reduction even for a strong load reduction (ca. 30% of design load), thus underlining how turbine maintains good performance for a wide range of operating conditions.

Table 4 Cycle parameters change for two representative off-design cases (CASE A, CASE B) respect to the design case (DESIGN).

Cycle Parameters			
	DESIGN	CASE A	CASE B
Inlet seawater temperature WW/CW, °C	28.00/4.00	28.00/4.00	24.00/7.00
Seawater mass flow rate WW/CW, kg/s	8798/8500	4399/4250	6920/6092
Net power output, MW_e	2.35	1.95	0.71
System net efficiency,	0.0205	0.0200	0.0085
Outlet seawater temperature WW/CW,°C	24.89/7.26	22.66/9.57	21.04/10.39
Global heat transfer coeff. EVA/COND, $kW/m^2/K$	4019/3465	3279/2672	3801/2803
Evaporation temperature, °C	22.05	20.37	19.00
Condensation temperature, °C	10.12	12.07	12.88
Pressure ratio,	1.483	1.314	1.224
Ammonia mass flow, kg/s	93.16	79.37	68.94
Turbine isentropic efficiency,	0.890	0.898	0.878

The off-design trends outlined in Table 4 are complemented by the representation of the thermodynamic cycles shown in Figure 7 together with cold (blue lines) and warm (red lines) seawater stream while thermodynamic cycle is reported in green. Gradient colors order follows the net power output trend.

This is a preprint of the following article:
Giostri, A., Romei, A. & Binotti, M., "*Off-design performance of closed OTEC cycles for power generation*", Renew. Energy, 2021.
The published article may differ from this preprint, and is available at the following DOI: 10.1016/j.renene.2021.02.047.

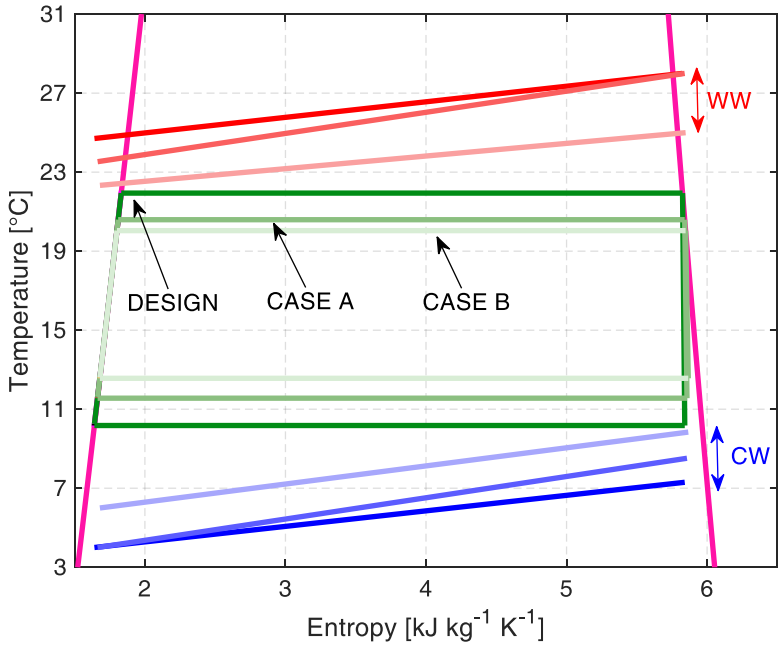

Figure 7 Ammonia cycles thermodynamic in Temperature-entropy space for the three cases reported in Table 4. Warm and cold seawater temperature variations are reported as well (entropy is properly scaled in order to match the corresponding ammonia entropy).

Taking into account T_{ww} and T_{cw} equal to 24°C and 7°C respectively (CASE B), Figure 8(a) highlights the importance of choosing the seawater mass flowrates that maximize the net power output. In this specific case, the best performance is obtained for a reduction of approximately 30% of both mass flow rates.
Figure 8(b) reports, for $m_{ww,ratio}$ equal to 0.7, the trade-off described above highlighting the link between cold seawater mass flow rate and seawater pumping power, net cycle power output and cycle efficiency. It is possible to notice how an increase of cold seawater mass flow rate causes a decrease of cold seawater temperature difference (ΔT_{cw}) while the condenser minimum temperature difference ($\Delta T_{pp,cond}$) shows a slight increase hence, a reduction of condensing pressure can be appreciated and so higher cycle conversion efficiency is achieved. On the contrary, seawater pumping power is monotonically increasing with seawater mass flow rates, hence, the net power output (graphically shown by the difference of the two series) shows a maximum. The trends for a variation of warm seawater mass flow rates are analogous from a qualitative point of view.

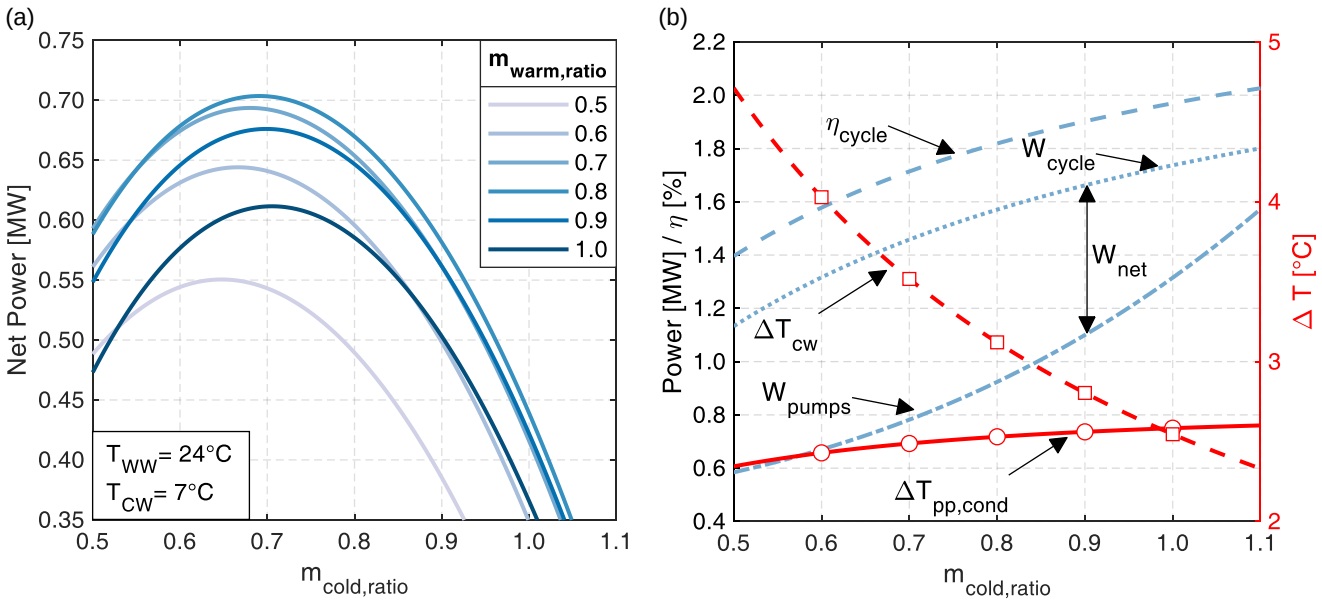

Figure 8 Effect of mass flow rates control on net power output for CASE B (T_{ww}=24°C, T_{cw}=7°C) (a). For CASE B ($m_{warm,ratio}$ equal to 0.7), seawater pumps consumption, net power output and efficiency of the cycle. Trend of cold seawater temperature difference and ΔT_{pp} of condenser (red series) is referred to secondary axis.

This is a preprint of the following article:
Giostri, A., Romei, A. & Binotti, M., "*Off-design performance of closed OTEC cycles for power generation*", Renew. Energy, 2021.
The published article may differ from this preprint, and is available at the following DOI: 10.1016/j.renene.2021.02.047.

In order to reduce the computational efforts requested by a yearly simulation and to give a single view the results described above, an operational map that shows the maximum power output achievable by the OTEC plant as a function of the exogenous parameters is computed and reported in Figure 9. Specifically, for each value of cold and warm seawater temperature the maximum electric net power achievable (varying both the seawater mass flow rates) is reported hence, each reported value represents the highest net power output as shown in Figure 8(b). The performance map contains system efficiency too.
Interpolating (bi-linearly) the operational map with seawater temperatures data makes it possible to perform fast simulation while keeping a satisfactory level of accuracy.

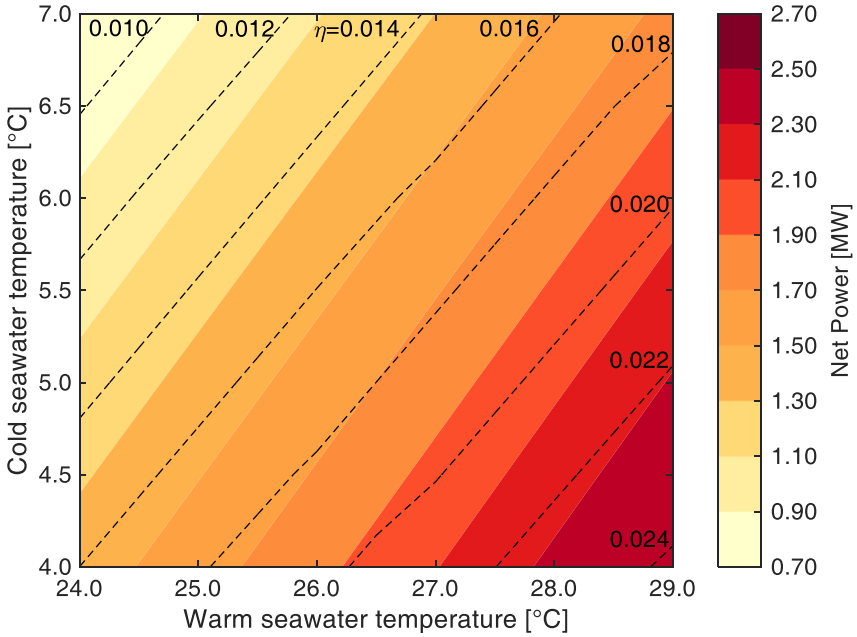

Figure 9 Optimized OTEC system net power output and corresponding efficiency (dashed lines) as function of cold and warm seawater temperatures.

5 Yearly electricity output

The part-load model described before is adopted to estimate the maximum annual electricity yield of the OTEC plant once the time series of seawater temperatures are available.
The Hawaiian Islands are universally recognized as a favorable location for OTEC plant thanks the high available temperature difference between surface and deep seawater coupled with the presence of a considerable electricity demand (about 9.7 TWh [42]) that currently is fulfilled for more than 70% by imported petroleum and coal thus causing the highest electricity price among U.S states [42].
The Hawaiian Islands are thus selected as location for the yearly analysis.
Superficial seawater temperature data, sampled with 15 minutes timestep, are retrieved from the National Data Buoy Center website [21], while a constant value of 4°C for the temperature of deep seawater is assumed as no information on its temperature is available. Deep water temperature is naturally less variable but, in some locations, internal waves can be responsible of short-term temperature variations that could impact on plant performance.
It is worth underlining that the seawater temperature data have to be considered as indicative and they do not replace a dedicated measurement campaign that is of paramount importance to correctly evaluate the OTEC potential while avoiding the presence of local seawater temperature anomalies.
Figure 10 (a) shows the annual profile of warm seawater temperature considered in this study while Figure 10 (b) reports the monthly average temperature of warm seawater along with the monthly maximum and minimum temperature. Figure 10 (c) shows a part of Hawaiian Islands chart together with the bathymetry.

This is a preprint of the following article:
Giostri, A., Romei, A. & Binotti, M., "*Off-design performance of closed OTEC cycles for power generation*", Renew. Energy, 2021.
The published article may differ from this preprint, and is available at the following DOI: 10.1016/j.renene.2021.02.047.

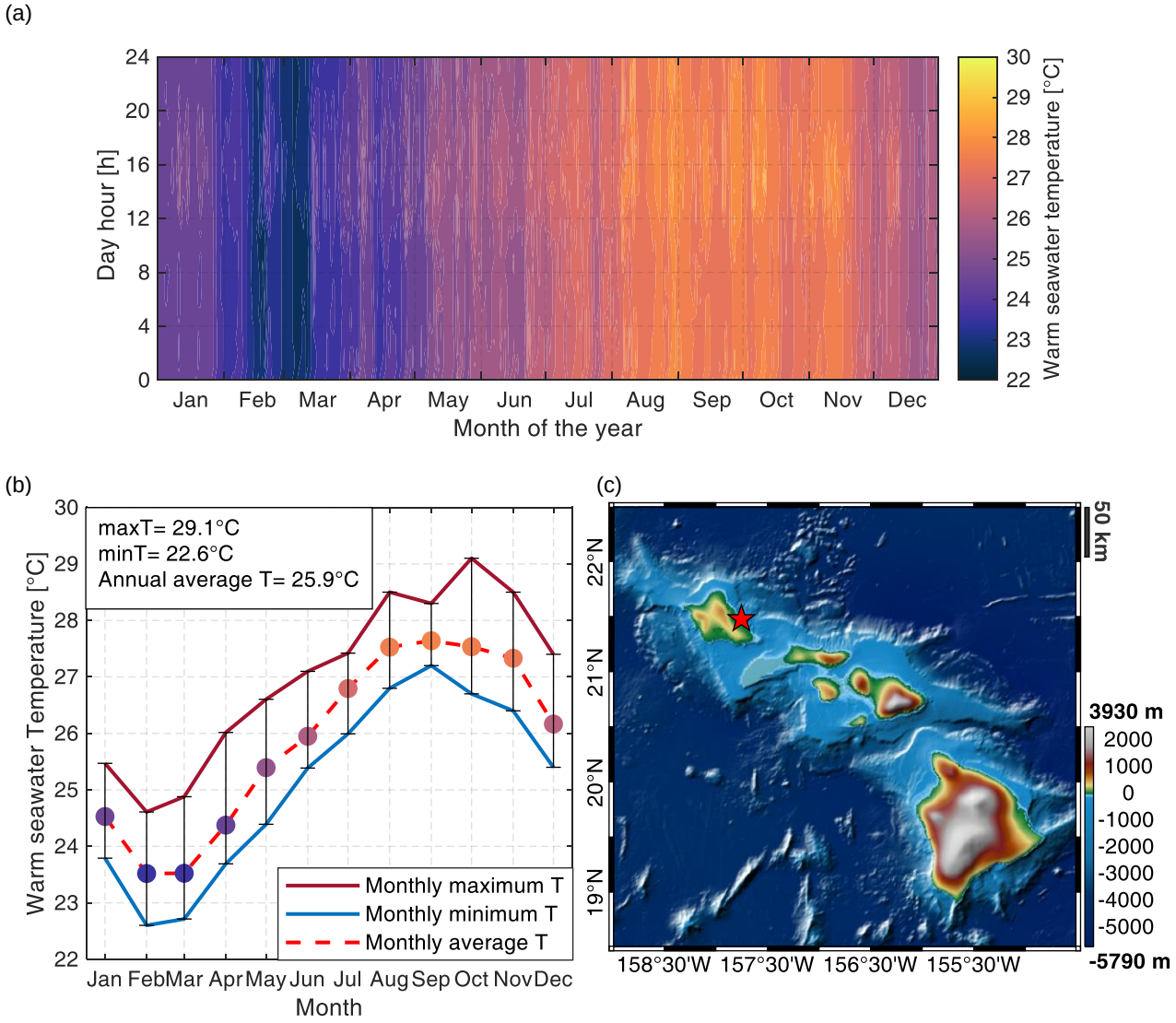

Figure 10 Annual surface seawater temperature (Station 51207) with a time stamp of 15 minutes (a) and monthly average surface seawater temperature (b). Fraction of Hawaiian Islands cart with bathymetry highlighted (c).

Upon examination of Figure 10 (b), it is worth to notice how the selected location is characterized by a significant change of surface seawater temperature, ranging from 29.1°C to 22.6°C (annual average temperature is equal to 25.9°C), thus justifying the need for a dedicated off-design model in order to obtain a reliable estimate of the yearly electricity yield. Once the exogenous parameters are defined, the yearly electricity yield is computed using the off-design map previously computed (see Figure 9).

The obtained result for 8000 equivalent hours is of 15.963 GWh_e, appreciably lower (18%) with respect to the result previously published, in which a constant warm seawater temperature (equal to 28°C was assumed).
As widely reported in Open Literature, LCOE is a valuable parameter to compare power generation technologies. Taking into account the components investment costs along with the annual electricity yield, LCOE is estimated to be equal to 316 €/MWh_e [c]. Table 5 summarizes the cost main assumptions considered to estimate the plant investment cost.

Table 5 Component cost estimates for the optimized power plant [44-46].

Investment Cost	
Component	**Costs**
Evaporator	869 €/m^2
Condenser	869 €/m^2
CWP	590 k€/$(m^3/s)_{cold,sw}$

[c] FCR (Fixed Charge Rate) equal to 10.05%: FCR is the interest rate needed to cover the capital cost, a return on debt and equity, and various other fixed charges [43].

This is a preprint of the following article:
Giostri, A., Romei, A. & Binotti, M., "*Off-design performance of closed OTEC cycles for power generation*", Renew. Energy, 2021.
The published article may differ from this preprint, and is available at the following DOI: 10.1016/j.renene.2021.02.047.

Turbogenerator	442 €/$kW_{e,turbine}$
Warm seawater pump	890 €/$kW_{e,pump}$
Cold seawater pump	890 €/$kW_{e,pump}$
Operation and maintenance [% Plant Cost]	3.3
Other costs	26% of components cost
Engineering and project management	4076 €/$kW_{e,net}$
Total Investment Cost	15518 €/ $kW_{e,net}$

5.1 System design optimization

Once the complete OTEC model is presented and discussed for a given plant design (see Paragraph 3), the question that naturally arises is which is the optimum design that minimizes the LCOE.
In order to answer this point, a series of OTEC plants, which differ in both the design warm seawater temperature and design cold seawater mass flow rates, are sized with the model described in [8]. It is worth to underline that all the considered OTEC plants have the same CWP diameter, namely 2.5 m and, accordingly, its investment cost is maintained equal to the reference case (8500 kg/s, 4°C) for each investigated design.
From a rigorous point of view, the ammonia expander should be re-designed for each studied design thus originating different performance maps (see 4.1.2).
Nevertheless, the limited change of size parameter (0.2 m – 0.4 m) and expansion ratio (1.43 – 1.5) allow maintaining, as a first approximation, the dimensionless expander performance map obtained in section 4.1.2. As regards the isentropic efficiency, it can be assumed that 89.2% can be attained by varying the rotational speed with the addition of a gearbox or an inverter. It is worth to underline that the addition of an inverter allows maximizing the turbine isentropic efficiency in off-design condition at an additional investment cost.
Keeping the assumptions reported in Table 1, cold water mass flow and design warm water temperature are varied and, among all possible sizing configuration represented by optimization variables (i.e. T_{cw},T_{ww}, $\Delta T_{pp,ww}$, $\Delta T_{pp,cw}$, v_{HX}), the design tool identifies the set that guarantees the higher γ (read the lowest specific investment cost). Conscious that this sizing choice is not rigorous, because it does not exactly guarantee to attain the lowest LCOE, it is a design approach useful to explain the main concept.
For each selected design, the procedure described in the previous sections is considered and the LCOE is computed.
Figure 11 shows the LCOE obtained for different plant designs in terms of warm seawater temperature and cold seawater mass flow rate for the Hawaiian Islands case. The iso-specific investment cost lines are drawn (black dashed lines) and both the minimum LCOE, specific to the best sizing (red pentagram) and the LCOE of the design reported in section 3 (grey circle) are highlighted as well.

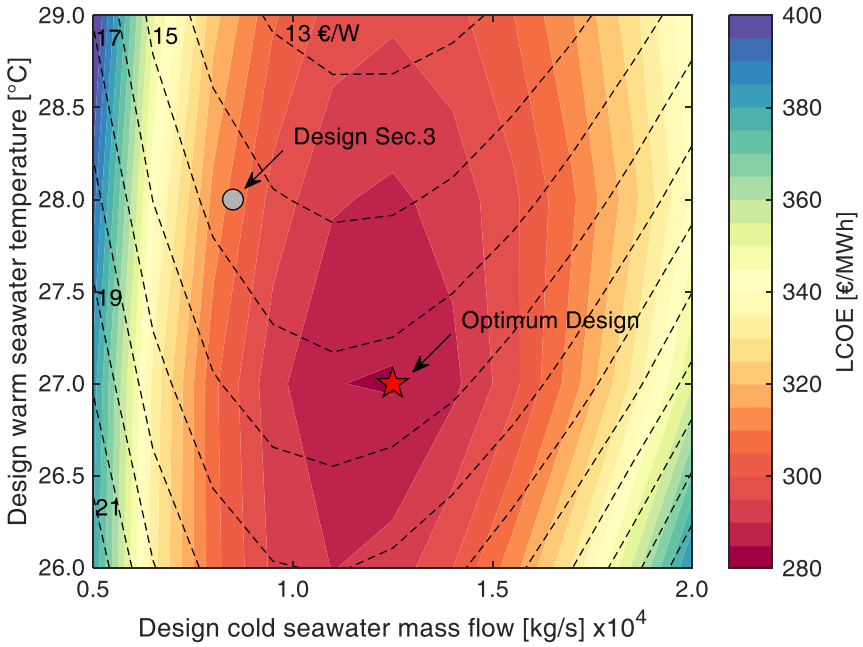

Figure 11 LCOE of different designs that differs in both design warm seawater temperature and design cold seawater mass flow rate. Iso-specific investment cost lines are reported.

It is worth to notice how the LCOE trend is quite flat near the minimum of 284 €/MWh_e is obtained for a design warm seawater temperature and cold seawater mass flow rates of 27°C and 12500 kg/s, respectively. The corresponding design net power output is equal to 4066 kW_e and the yearly electric energy yield is equal to 30.3 GWhe. The LCOE estimate is strongly affected by uncertainty in components investment cost, but the best design parameters (i.e. warm seawater

This is a preprint of the following article:
Giostri, A., Romei, A. & Binotti, M., "*Off-design performance of closed OTEC cycles for power generation*", Renew. Energy, 2021.
The published article may differ from this preprint, and is available at the following DOI: 10.1016/j.renene.2021.02.047.

temperature, cold seawater mass flow) are nearly independent of it. Figure 12(a-b) shows the impact of the design cold seawater mass flow rate on the main system parameters for a fixed design warm seawater temperature (i.e. 27°C). Specifically, Figure 12(a) confirms the presence of a minimum LCOE resulting from the different rate of increase of both plant investment cost (dominated by heat exchangers and CWP) and the annual electricity yield that naturally follows the increase of nominal net power. It is possible to notice that CWP investment cost is maintained equal for each design. Figure 12 (b) shows the nominal net power, obtained as the difference between the cycle power output and the seawater pumps consumption. The simile-parabolical pumping power increase (see sections 4.2-4.3) penalizes the net power output that decreases after reaching a maximum at higher mass flow. The specific investment cost is characterized by a trend similar to the LCOE while a completely different trend of γ parameter can be appreciated. This discrepancy is produced by investment size-independent costs, such as CWP and engineering costs which are not included in the calculation of γ. This fact suggests how this parameter is not a figure-of-merit that exhaustively help to identify the optimum plant configuration when the study is focused on constant size CWP.

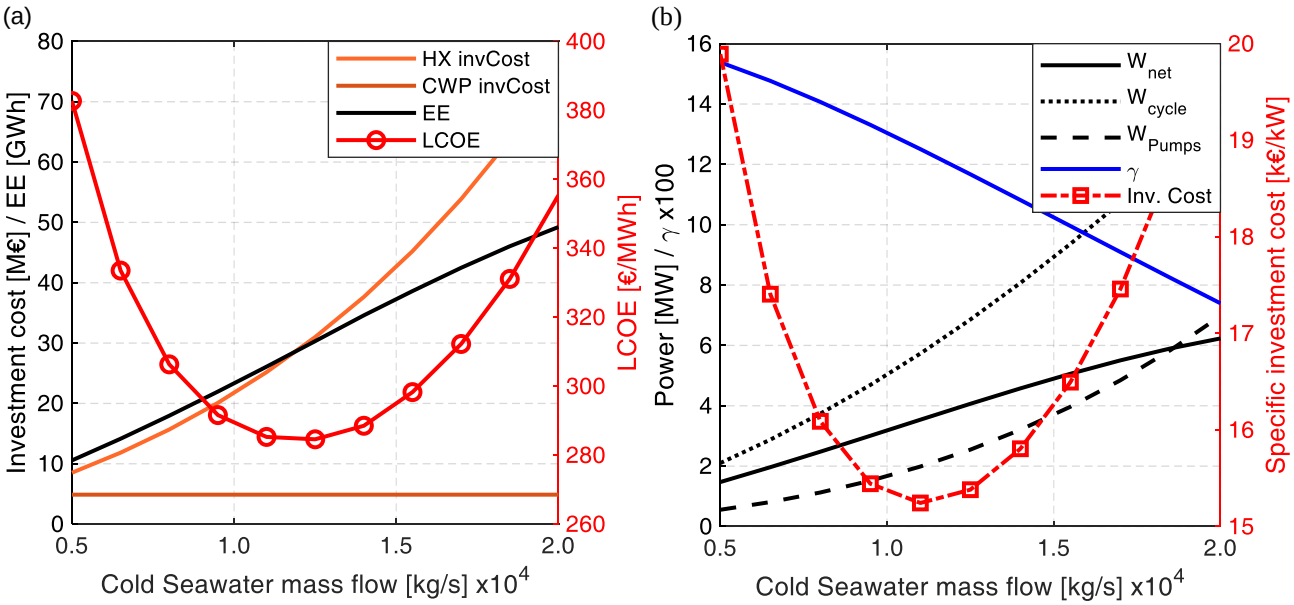

Figure 12 (a) Trends of HX and CWP investment cost together with year electricity yield for different design cold mass flow at same warm seawater temperature (27°C). LCOE is reported on secondary axis. (b) Nominal net power, gross cycle power and seawater pumps power, γ. Specific investment cost is reported on secondary axis.

Table **6** shows the off-design behavior for a plant designed to have the lowest LCOE (BEST). CASE A* and CASE B* are defined coherently with CASE A and CASE B in Table 1. It can be appreciated how the optimized design is characterized by a higher ratio between warm and cold seawater mass flow rates, with a significant increase of the net power output (+73%). This effect can be explained by the superior "energetic cost" associated to the exploitation of the cold seawater with respect to the warm seawater. As regards the off-design behavior, the observed trends are consistent with the ones reported in Table 1.

Table 6 Cycle parameters change for two representative off-design cases (CASE A*, CASE B*) with respect to the best design (BEST) identified above.

Cycle Parameters			
	BEST	CASE A*	CASE B*
Inlet seawater temperature WW/CW, °C	27.00/4.00	28.00/4.00	24.00/7.00
Seawater mass flow rate WW/CW, kg/s	16767/12500	8384/6250	13972/8750
Net power output, MW_e	4.06	3.46	1.45
System net efficiency,	0.0201	0.0196	0.0093
Outlet seawater temperature WW/CW,°C	24.11/7.92	22.90/12.75	21.28/11.37
Global heat transfer coeff. EVA/COND, $kW/m^2/K$	3036/2935	2421/2227	2893/2393
Evaporation temperature, °C	21.61	20.76	19.37
Condensation temperature, °C	10.10	12.75	13.26

This is a preprint of the following article:
Giostri, A., Romei, A. & Binotti, M., "*Off-design performance of closed OTEC cycles for power generation*", Renew. Energy, 2021.
The published article may differ from this preprint, and is available at the following DOI: 10.1016/j.renene.2021.02.047.

Pressure ratio,	1.4621	1.30	1.222
Ammonia mass flow, kg/s	164.02	139.13	127.68
Turbine isentropic efficiency,	0.890	0.898	0.885

5.2 CWP length optimization

As final analysis, an assessment of the influence of the CWP length on the LCOE is presented in the following. Taking into account the dependence of the cold seawater temperature on depth, it is possible to predict the presence of an optimal CWP length which represents the best trade-off between CWP investment cost, pumping power consumption and thermodynamic efficiency. It is important to underline that this kind of analysis is extremely influenced by both the shape of seawater thermocline and the bathymetric profile of the chosen site. In this preliminary analysis, the CWP length is computed by assuming a constant bathymetric slope (approximately 19°) and a CWP investment cost proportional to length.
Taking into account the temperature-depth profile reported in [47], which can be consider representative of the simile-Hawaiian site, the LCOE for cold seawater depths between 600 and 1400 m is computed. The computed LCOEs are obtained identifying for every depth a different design which minimizes the LCOE taking into account the variability of the warm seawater temperature reported in Figure 10.
Figure 13 reports the resulting LCOE, showing how, with the given set of assumptions, the decrease of CWP investment cost and seawater pumping consumption obtainable with shorter CWP does not counterbalance the reduction of cycle efficiency induced by the increase of cold seawater temperature.

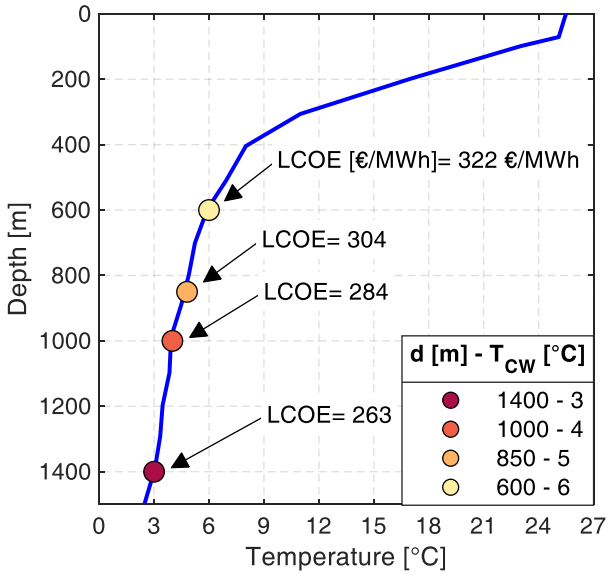

Figure 13 LCOE for different cold seawater depth (Temperature-depth profile adapted from [47]).

Far from being a rigorous rule, the trend of LCOE is influenced by the temperature-depth profile that is strongly site-dependent; in particular, it is possible to access to data obtained from floating buoys in the oceans that reports temperature-depth profile (till 2000 m) that confirms the need to a careful estimate of the cold seawater availability [48].

6 Conclusions and future developments

This work discusses a techno-economic assessment of a CC-OTEC (based on ammonia saturated Rankine cycle) with a particular attention posed on the description and analysis of a simulation tool able to predict the off-design behavior.
With the aim of filling a gap in OTEC system modelling, specific care is devoted to study the ammonia turbine. Turbine sizing is accurately performed by a mean-line code while the operating performance maps are obtained by mean of CFD simulations; in particular, specific analytical correlations, which explains the turbine off-design performance map, are deducted and proposed.
As a first analysis, OTEC plant that implements CWP with diameter equal to 2.5 m (reasonably considered as the current technological limit) is considered and the design characteristics are taken from a previously published work. For a specific location (i.e. Hawaii) characterized by a variable warm seawater temperature, the off-design model allows estimating the annual electricity yield and the corresponding LCOE, equal to 15.963 GWh_e and 316 €/MWh_e respectively; this LCOE is 18% higher with respect to the value estimated assuming a constant warm seawater temperature. The obtained LCOE is undoubtedly far from being competitive with conventional power generation technologies but, it results comparable (if not lower) with electricity price in remote islands, where thus the OTEC technology can be potentially implemented and further developed.

This is a preprint of the following article:
Giostri, A., Romei, A. & Binotti, M., "*Off-design performance of closed OTEC cycles for power generation*", Renew. Energy, 2021.
The published article may differ from this preprint, and is available at the following DOI: 10.1016/j.renene.2021.02.047.

Using the LCOE as objective function, the optimization of the design conditions is performed (i.e. cold mass flow rate and warm seawater temperature) thus extending what reported by the authors in a previous work. For the selected site, the best design is obtained for 12500 kg/s and 27°C, corresponding to LCOE reduction of 11% (284 €/MWh$_e$).
Since the objective functions (LCOE), near the optimum, results quite flat, a certain safe margin is available for OTEC plant design. It is worth to underline that the techno-economic assessment depends on site choice and it is affected by an unavoidable uncertainty that is mainly concentrated in the economic estimate of components investment costs that can affect the LCOE estimate. The significant cost uncertainty is unavoidably related to the lack of a significant OTEC market: a reduction of this uncertainty is anyhow reasonably foreseen thanks to the growing interest in the OTEC technology and thanks to the experience gained during real plants construction.
A sensitivity analysis on the CWP length for a given seawater temperature-depth profile has shown that the CWP cost reduction and the pumping power reduction obtainable with shorter CWP does not counterbalance the decay in the thermodynamic cycle efficiency.
Thanks to the capability of the developed suite (i.e. sizing and off-design performance), an interesting future development is represented by the study of the optimum OTEC plant in a scenario characterized by both variable electricity price and load request by the users. Moreover, the integration of OTEC plant inside microgrid, where different renewables (i.e. PV, wind etc.) can coexist together with storage systems (i.e. batteries, PHES etc.) [49,50], can enhance the opportunity for OTEC technology to penetrate the market of power generation in remote islands archipelagos.

7 References

[1] NASA (Global CLimate Change). Scientific Consensus: Earth's Climate is Warming 2020;2020.
[2] COP21 Website. COP21 website: http://www.cop21.gouv.fr/en/;2016.
[3] Rogelj J, Den Elzen M, Höhne N, Fransen T, Fekete H, Winkler H, et al. Paris Agreement climate proposals need a boost to keep warming well below 2°C. Nature 2016;534:631-639.
[4] Pelc R, Fujita RM. Renewable energy from the ocean. Mar Policy 2002;26:471-479.
[5] IRENA. Renewable power generation costs in 2018. International Renewable Energy Agency 2019.
[6] International Renewable Energy Agency. Ocean thermal energy conversion: technology brief. IRENA Ocean Energy Technology Brief 2014.
[7] Global CCS Institute. Energy use in the Pacific region 2013; 2017.
[8] Bernardoni C, Binotti M, Giostri A. Techno-economic analysis of closed OTEC cycles for power generation. Renewable Energy 2019;132:1018-1033.
[9] Zhang X, He M, Zhang Y. A review of research on the Kalina cycle. Renewable and sustainable energy reviews 2012;16:5309-5318.
[10] Sun F, Ikegami Y, Jia B. A study on Kalina solar system with an auxiliary superheater. Renewable Energy 2012;41:210-219.
[11] Bharathan D. Staging Rankine Cycles Using Ammonia for OTEC Power Production‖, Nat. Renewable Energy Laboratory, Golden, CO, Rep.NREL/TP-5500-49121 2011.
[12] Ikegami Y, Uehara H. Thermodynamic Optimization in Ocean Thermal Energy Conversion. In: Anonymous Thermodynamic Optimization of Complex Energy Systems, Springer; 1999, p. 335-344.
[13] Yang M, Yeh R. Analysis of optimization in an OTEC plant using organic Rankine cycle. Renewable Energy 2014;68:25-34.
[14] Mathworks®. Mathworks webpage, http://www.mathworks.com/ 2018.
[15] Uehara H, Ikegami Y. Optimization of a closed-cycle OTEC system. J Sol Energy Eng Trans ASME 1990;112:247-256.
[16] Yang MH, Yeh RH. Analysis of optimization in an OTEC plant using organic Rankine cycle. Renew Energy 2014;68:25-34.
[17] Lemmon EW, Huber ML, McLinden MO. NIST Standard Reference Database 23: Reference Fluid Thermodynamic and Transport Properties-REFPROP, Version 9.1, National Institute of Standards and Technology, Standard Reference Data Program, Gaithersburg, 2013.
[18] Tillner-Roth R, Harms-Watzenberg F, Baehr HD. A new fundamental equation for ammonia; Eine neue Fundamentalgleichung fuer Ammoniak 1994.
[19] McDougall TJ, Barker PM. 2011: Getting started with TEOS-10 and the Gibbs Seawater (GSW) Oceanographic Toolbox
. SCOR/IAPSO WG127 2011.
[20] Okinawa Prefecture. Ocean Thermal Energy Conversion on Kume Island, Okinawa, Japan 2017;2017.
[21] National Oceanic and Atmospheric Administration. National Data Buoy Center's 2020;2020.
[22] Keesmaat K. Installation Limits of Large Diameter Cold Water Pipes in Deep Water for Land-Based OTEC Plants 2015.
[23] Hindmarsh AC, Brown PN, Grant KE, Lee SL, Serban R, Shumaker DE, et al. SUNDIALS: Suite of nonlinear and differential/algebraic equation solvers. ACM Transactions on Mathematical Software (TOMS) 2005;31:363-396.
[24] Serban R. SundialsTB v. 2.4.0, a Matlab interface to SUNDIALS 2012.

[25] Ennio Macchi, Marco Astolfi. Organic Rankine Cycle (ORC) Power Systems Woodhead Publishing Ltd: GB; 2016.
[26] Pini M, Persico G, Casati E, Dossena V. Preliminary design of a centrifugal turbine for organic rankine cycle applications. Journal of Engineering for Gas turbines and power 2013;135:042312.
[27] Dixon SL, Hall C. Fluid Mechanics and Thermodynamics of Turbomachinery Butterworth-Heinemann; 2013.
[28] Kostors CH, Vincent SP. Ammonia turbine design for Ocean Thermal energy Conversion (OTEC) plants. J Sol Energy Eng Trans ASME 1981;103:92-97.
[29] Storn R, Price K. Differential evolution–a simple and efficient heuristic for global optimization over continuous spaces. J Global Optimiz 1997;11:341-359.
[30] ANSYS. ANSYS-CFX website: https://www.ansys.com/products/fluids/ansys-cfx/ansys-cfx-features; 2020.
[31] Menter F. Zonal two equation kw turbulence models for aerodynamic flows 1993:2906.
[32] Lettieri C, Paxson D, Spakovszky Z, Bryanston-Cross P. Characterization of nonequilibrium condensation of supercritical carbon dioxide in a de laval nozzle. Journal of Engineering for Gas Turbines and Power 2018;140:041701.
[33] Gyarmathy G. Nucleation of steam in high-pressure nozzle experiments. Proc Inst Mech Eng A: J Power Energy 2005;219:511-521.
[34] Baltadjiev ND, Lettieri C, Spakovszky ZS. An Investigation of Real Gas Effects in Supercritical CO2 Centrifugal Compressors. Journal of Turbomachinery 2015;137:091003-13.
[35] AspenTech. Aspen Exchanger Design & Rating ("EDR") 2013.
[36] Cooper MG. Heat Flow Rates in Saturated Nucleate Pool Boiling-A Wide-Ranging Examination Using Reduced Properties. Advances in Heat Transfer 1984;16:157-239.
[37] Cooper MG. Saturation Nucleate Pool Boiling - a Simple Correlation. In: Simpson HC, Hewitt GF, Boland D, Bott TR, Furber BN, Hall WB, et al. First U.K. National Conference on Heat Transfer, Pergamon; 1984, p. 785-793.
[38] Kakaç S, Liu. Heat Exchangers: Selection, Rating, and Thermal Design, Third Edition CRC Press: Hoboken; 2012.
[39] Avery WH, Wu C. Renewable Energy from the Ocean. A Guide to OTEC Oxford University Press: New York; 1994.
[40] Avery WH. Ocean thermal energy conversion (OTEC).
[41] Thermoflow Inc. Thermoflex v.24 User Guide, https://www.thermoflow.com/ 2014.
[42] U.S. Energy Information Administration (EIA). Energy Information Administration - EIA - Official Energy Statistics from the U.S. Government. 2020;2020.
[43] Kreith F, Krumdieck S. Principles of Sustainable Energy Systems, Second Edition Taylor \& Francis; 2013.
[44] Lemmens S. Cost engineering techniques and their applicability for cost estimation of organic rankine cycle systems. Energies 2016;9.
[45] Upshaw CR. Thermodynamic and economic feasibility analysis of a 20MW Ocean Thermal Energy Conversion (OTEC) power plant 2012.
[46] Lockheed Martin. NAVFAC Ocean Thermal Energy Conversion (OTEC) Project. Configuration Report and Development Plan for 2.5MW OTEC Mini-Spar Pilot Plant 2011.
[47] Kobayashi K, Jitsuhara S, Uehara H. The present status and features of OTEC and recent aspects of thermal energy conversion technologies 2004.
[48] Argo. Argo float data and metadata from Global Data Assembly Centre (Argo GDAC) 2020.
[49] Grazzini G, Milazzo A. Thermodynamic analysis of CAES/TES systems for renewable energy plants. Renewable Energy 2008;33:1998-2006.
[50] Fossati JP, Galarza A, Martín-Villate A, Fontán L. A method for optimal sizing energy storage systems for microgrids. Renewable Energy 2015;77:539-549.